Performance of Hybrid Castellated Beams

Prediction Using Finite Element Modeling

Wael A. Salah
Civil Engineering Department
College of Engineering, Northern Border University
Arar, Saudi Arabia
and
Civil Engineering Department
Faculty of Engineering, Al Azhar University
Cairo, Egypt
wael.khalil@nbu.edu.sa

Received: 12 February 2022 | Revised: 28 February 2022 | Accepted: 2 March 2022

Abstract-In the current study, the up to failure behavior of the Hybrid Castellated Beams (HCBs) is predicted with the use of a developed Finite Element (FE) model. Both material and geometric nonlinearities are considered in the numerical simulations. The accuracy of the FE model was validated using the experimental test results presented in the literature. The results of the FE analysis had a close agreement with the experimental work in predicting the failure load and failure mode pattern. A parametric study was conducted to investigate the influence of some parameters on HCBs' ultimate strength. These parameters included slenderness of compression flange, beam span-to-depth ratio, and laterally unbraced length of compression flange. A design formula is proposed to estimate the inelastic lateral-distortional strength of both homogeneous and hybrid material castellated beams.

Keywords-castellated beams; finite element analysis; failure load; lateral-distortional; unbraced length; slenderness

I. INTRODUCTION

Beams with web openings have been widely involved in various large-scale steel structure projects such as hyper markets, car parking buildings, and storage facilities. The economic cost and the authentic appearance in addition to the provided facility to pass the services through web openings, have encouraged the designers to involve these opened-web steel elements in their designs. The utmost number of carried out researches on hot-rolled steel elements are directed to plain-web elements either in a simple beam or in a frame system as presented in [1-5]. On the other hand, during the last two decades, extensive studies focused on the investigation of the performance of perforated-web beams fabricated from hot-rolled elements. Many researchers focused on the determination of the loading capacity of bar steel opened-web beams [6-12] and steel-concrete composite opened-web beams [13-17], whereas the possible instability failure modes of perforated-web beams were highlighted in [18-22].

Recently, various endeavors have been made to improve the performance of steel beams. One of these efforts was to increase the depth of the I-profile steel beam by cutting its web in a special pattern and re-welding the two split parts to form what is known as the Castellated Beam (CB) or perforated-web beam. The load strength of CBs could be increased by utilizing a higher-grade steel material for the entire beam. However, higher-grade steel can be specified only for certain parts of the steel beam forming what is known as a hybrid beam. Commonly, higher-grade steel is used for flanges whereas relatively lower-grade is used for web plates. Since CB is a combination of two welded rolled beam halves, it is very convenient to combine two alternate halves from two different rolled beams, each with a specific steel grade to form an HCB. This method causes no losses of steel materials and, in the same time, may raise the CB load strength. Concerning hybrid steel beams, most of the carried out studies focused on the performance of hybrid solid-web beams [23-26]. A simple design formula was suggested to determine the bending resistance of hybrid beams in [27]. The flexure strength and the ductility of hybrid high-performance beams, have been evaluated in [28]. An analytical method for determining the biaxial bending stress through the unsymmetrical hybrid beams was proposed in [29]. The distortional buckling capacity of built-up-cold-formed hybrid double-I-box beams was experimentally and numerically investigated in [30]. Furthermore, it has been demonstrated that the flexure strength, rotation capacity, and failure mode pattern of a simply supported hybrid beam are substantially affected by the applied moment, whether gradient or uniform [30]. One of the earlier recorded research projects in HCBs, was [31]. In that study, hybrid beams with one rectangular web opening at mid-span failed due to the flexural deformation. After a while, the same researchers introduced an analytical solution for calculating the bending strength of both homogeneous and HCBs [32]. However, less attention, if any, has been paid in reviewing the performance of HCBs fabricated by welding two halves of I-profile beams with different grade materials.

This study focuses on the evaluation of the load strength of HCBs formed from two I-profile beams of different steel grades. FE analysis was utilized to investigate the behavior of HCBs. The developed FE model was calibrated with the experimental results from the relevant literature. The results of the FE model agree with the experimental results. This gave a

Corresponding author: Wael A. Salah

strong confidence to employ the validated FE model in predicting the ultimate load strength of HCBs. Furthermore, the developed FE model has been utilized to apply a parametric study to examine the effect of certain parameters on the strength of HCBs. The considered parameters were slenderness ratio of compression flange, beam-span-to-depth ratio, and laterally unbraced length of compression flange.

II. FINITE ELEMENT MODELING

A 3D FE model was developed in ABAQUS [33], to study the behavior of CBs. Flanges, web, and support stiffeners of CBs were modeled using the four-node general-purpose doubly-curved shell elements with reduced integration, S4R. The mid-span point load was applied through a steel block of 100×100×40mm to avoid any kind of stresses concentration at the point of load application. The external steel block was modeled using C3D8R elements and it was connected to the top flange through the surface-to-surface contact option available in ABAQUS. Small sliding contact interface was applied between the bottom surface of the steel block and the top surface of the top flange and a 0.2 friction coefficient was applied between the two contacted surfaces. The end beam vertical support was modeled by restraining a line of nodes at the bottom flange, located at the beam end-support, from the translation in both vertical and lateral directions. The nodes of beam flanges, at a distance of 165mm from the end-support, were precluded against any lateral translation. The steel block was rigidly constrained to a reference point positioned at its top surface center. This assigned reference point was restrained not to move in the two horizontal directions. Both material and geometric nonlinearities were considered in the FE analysis. Steel was modeled as elastic-plastic with strain hardening. Young's modulus, E, of 210GPa and Poisson's ratio, ν, of 0.3 were used to model the elastic material behavior. The true stress-strain was considered to represent the material nonlinearity. The initial geometric imperfection was introduced to the FE model by scaling the first eigenmode obtained from the conducted elastic buckling analysis by a factor of L_b/1000, where L_b is the effective laterally unbraced length of the compression flange [34].

III. VALIDATION OF THE FINITE ELEMENT MODEL

In order to validate the developed FE model, the acquired FE results were compared to those of previously tested beams in the literature. Six simply supported beams tested in [22] were numerically simulated using the present FE model. The results of tensile coupon tests [22] were converted to true stress-strain values to represent the material nonlinearity behavior. Figure 1 depicts the conducted comparison between the results of FE analysis and the tested specimen C210-3600. The first and second numbers refer to the section height and beam's span length respectively. The results are presented in terms of load to lateral displacement. In the experimental program, the lateral displacements were recorded at three points along the mid-span section, namely T4, T5, and T6 to represent respectively top, middle, and bottom of the considered section. The developed deformations at the end of the experimental test and at the ultimate load of FE analysis of the specimen C210-4400 are compared in Figure 2. Table I exhibits the numerically and experimentally achieved ultimate loads for all tested specimens. The applied comparison indicates that the developed FE model can predict the ultimate load of all tested CBs. However, the relative discrepancy in tracing load to lateral-displacement relation in specimen C210-3600 attributes to the applied initial geometric imperfection at the beginning of the FE analysis. The partial lateral restrains provided by the friction developed between the surfaces of steel block and top-flange of the tested specimens should be added to that. The carried out validation for the developed FE model, gives a strong confidence to employ this FE model in a parametric study.

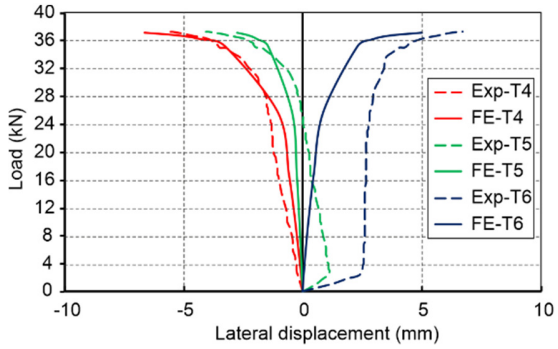

Fig. 1. Load-lateral displacement comparison (C210-3600).

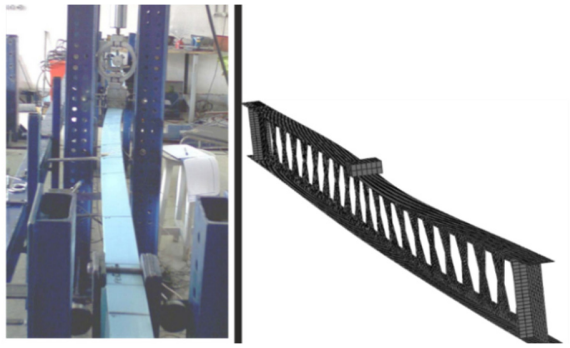

Fig. 2. Resulted deformations of specimen C210-4400 (a) at failure load through the test and (b) FE analysis.

TABLE I. FE ANALYSIS AND TEST RESULTS COMPARISON

Specimen	P_{test} (kN)	P_{FE} (kN)	P_{FE} / P_{test}
C180-3600	21.58	22.052	1.02
C180-4400	15.63	16.29	1.04
C180-5200	25.92[i]	12.926	0.499
C210-3600	37.22	37.69	1.01
C210-4400	39.94[ii]	29.788	0.746
C210-5200	24.9	25.198	1.01

[i] Initial geometric imperfections of this tested specimen resulted in a higher failure load than the expected value [22]. [ii] Observed developed frictional restraint at the loading point during the test, led to a higher beam strength compared to the other tested C210 beams [22].

IV. PARAMETRIC STUDY

The parametric study was carried out to scrutinize the performance of CBs fabricated from two different steel grades (hybrid beams). Hybrid steel I-beams, are usually built up from two flanges with a steel grade higher than that of web plate. CBs are typically fabricated from hot-rolled profile by welding two components, the top part (CBT) and the bottom part

(CBB). One of the economical alternatives to enhance CBs load carrying capacity, is to combine the two welded beam parts from two I-profiles with different steel grades. The current parametric study aims to investigate certain CB parameters such as the slenderness ratio of beam flanges, the span-to-depth ratio, and the length of unbraced compression flange on HCBs ultimate load. The suggested beam layout is shown in Figure 3 while the beam section, and the distribution of web openings are shown in Figure 4. The proposed CB was built up from the UB152×89×16 beam profile. Steel grades S275, S355, S420, and S460 [35] were adopted for the materials of numerically analyzed beams. Lateral horizontal displacement is completely restrained at the point of load application.

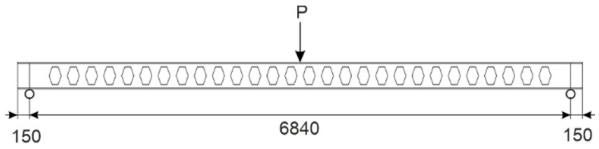

Fig. 3. Layout of FE analyzed castellated beam.

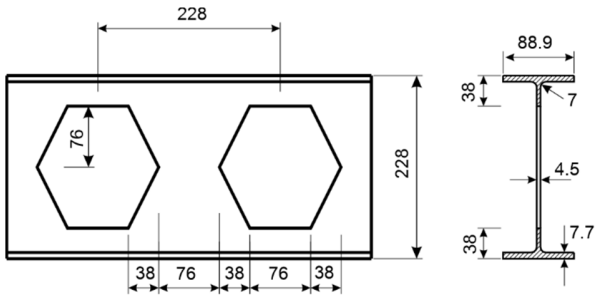

Fig. 4. Opening distribution and section details of an FE analyzed castellated beam.

A. Compression Flange Slenderness

The slenderness of compression flange has a great impact on the ultimate load of CBs. The effect of flange slenderness was examined numerically through 7 beam groups, with 4 CBs in each group. The CB groups were modeled. The beams in the first 3 groups were HCBs and homogeneous in the last 4 groups. Each group consisted of 4 beams: CB-1, CB-2, CB-3, and CB-4. Hybrid beams were formed from two halves, CBT and CBB, that appertained to two rolled I-profiles with different steel grades. For all hybrid beams, the material of CBB was always of grade S275, whereas steel grades S355, S420, and S460, were assigned to CBT of the hybrid beam groups, Gr-1, Gr-2, and Gr-3 respectively. Steel grades S275, S355, S420, and S460 were assigned, in order, as the material properties for the last 4 homogeneous beam groups, Gr-4, Gr-5, Gr-6, and Gr-7. The compression flange of all CBs was laterally restrained only at end supports and at beam mid-span point of load application. The results of CBs in the group Gr-4, homogeneous CBs of steel grade S275, were used to normalize the corresponding beam result within the other beam groups.

To study the effect of flange slenderness, λ_f, on the CB ultimate load, thickness values of 4, 6, 8, and 10mm were assigned to the CB flanges CB-1, CB-2, CB-3, and CB-4 respectively in each group from Gr-1 to Gr-7. The above assigned thickness values of beam flanges, resulted in slenderness ratios of 11, 7.4, 5.56, and 4.45 correspondingly. The lowest scaled eigenmode, picked up from the conducted eigenvalue buckling analysis, was introduced to each FE model typifying the initial geometric imperfection. Modified Riks method [28] was used to predict the nonlinear response of the CBs. The FE models' notation, i.e. All_S275, All_S355, All_S420, and All_S460 refer to the analyzed homogeneous beams with steel material grades of S275, S355, S420, and S460 in order, whereas the notations Top_S355, Top_S420, and Top_S460 refer to the FE models of HCBs with CBT assigned material grades of S355, S420, and S460 respectively.

The results of FE analysis are presented in Figures 5 and 6. Considering homogeneous CBs, it is conspicuous that using higher-grade steel, has increased CB ultimate load. However, the influence of the material grade has degraded as the compression flange slenderness increased. Likewise, specifying higher-grade material to CBT in HCBs, increased the ultimate strength of HCBs. Figures 5 and 6 clearly reflect that utilizing a higher-grade material, whether for the entire homogeneous beam or for the hybrid beam's top half, has almost the same effect on the beam's achieved ultimate strength. These results can be interpreted by investigating HCB stress distribution by approaching failure load. Figure 7 maps the von Mises stress distribution of HCB Top_460 at failure load. It can be observed that the beam failed in the instability mode of lateral torsional-distortional buckling. Hence, particular zones of the laterally displaced compression flange have achieved the yield stress whereas the stress in the bottom flange was still below yielding. Therefore, raising the limit of the yield stress of the beam's top-half, increased the entire castellated beam load strength. Hence, the failure load of the HCB is only controlled by the top compression flange. The analyzed HCBs with a steel grade S460 employed to CBT and with a flange slenderness ratio equal to 11, sustained more than 13% higher ultimate load compared to that of homogeneous beams with steel of grade S275. However, this gained load ratio was increased to 19% when the slenderness of the compression flange shifted to 4.45.

B. Span-to-Depth Ratio

Beam span-to-depth ratio plays a non-trivial impact on the CB strength. To examine the effect of span-to-depth ratio on the CB ultimate strength, 7 groups, Gr-8 to Gr-14, were numerically simulated. These beam groups are indistinguishable from the prior introduced groups, Gr-1 to Gr-7, in the same order considering the utilized materials, root I-profile, web openings distribution, and compression flange lateral restraints. The cross-section of all beams in this study part is invariant and matched to that of the original considered I-profile shown in Figure 4. The considered span-to-depth ratios for castellated beams CB-1, CB-2, CB-3, and CB-4 in the Gr-8 to Gr-1428 groups are 30, 32, and 34. Varying span-to-depth ratios were generated by changing the beam span length. The numerically achieved ultimate strengths of the homogeneous and hybrid beams with disparate span-to-depth ratios, are shown in Figures 8 and 9. The presented FE results show that a larger span-to-depth ratio leads to a lower beam ultimate strength for both homogeneous and hybrid beams with the same cross-section for all utilized steel grades. Since all

beams of this subsection have failed in the instability mode of lateral torsional-distortional buckling, the top flange has reached the yield stress earlier than the bottom flange. Thus, for all considered span-to-depth ratios, specifying a higher steel grade for the top-half of HCBs, resulted in greater ultimate load strength that could be attained before failure.

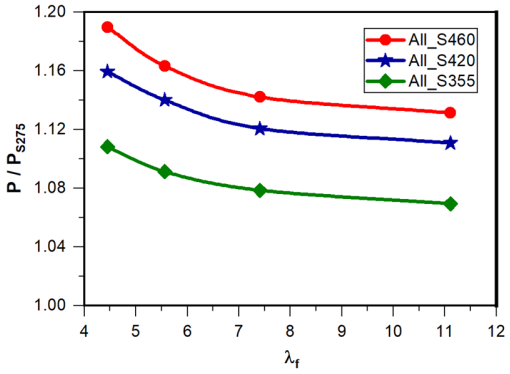

Fig. 5. Ultimate loads of homogeneous castellated beams with various values of flange slenderness.

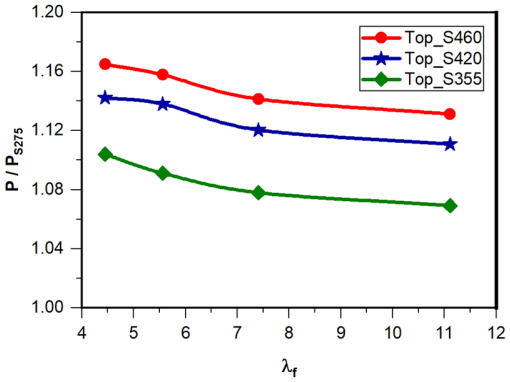

Fig. 6. Ultimate loads of hybrid castellated beams with various values of flange slenderness.

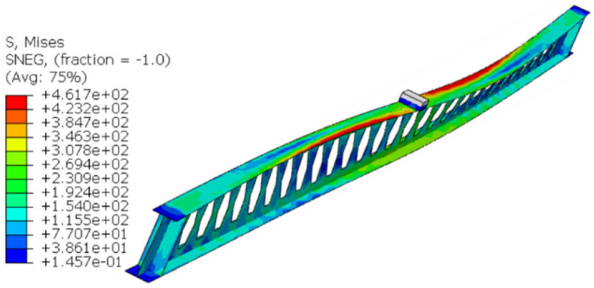

Fig. 7. Von Mises stresses distribution at failure load of analyzed HCB with λ_f=5.56, Top_S460.

C. Unbraced Length of Compression Flange

This part of the paper intends to study the effect of unbraced compression flange length (L_b) on the ultimate strength of HCBs. Two different arrangements of HCBs were considered. HCBs scrutinized types are: 1) higher-grade steel to be assigned to CBT, 2) higher-grade steel to be assigned to the castellated beam's flanges (CBFs).

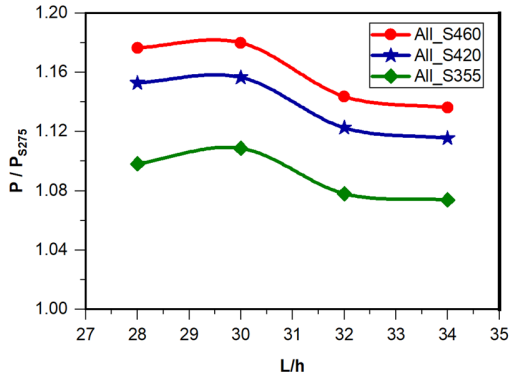

Fig. 8. Effect of span-to-depth ratio on the failure load of homogeneous castellated beams using various steel grades.

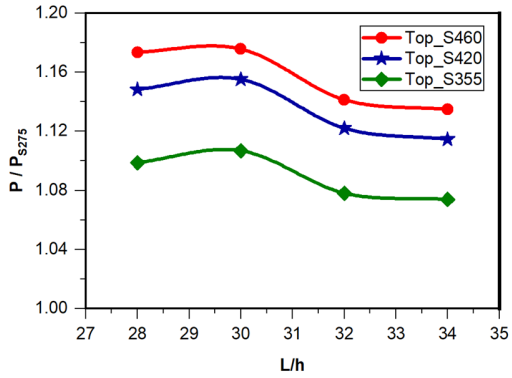

Fig. 9. Effect of span-to-depth ratio on the failure load of hybrid castellated beams considering various steel grade for the top-half beam section.

1) Applying Higher Grade Steel to the Top-half of the Castellated Beams

Seven groups of CBs, Gr-15 to Gr-21, identical to the earlier introduced Gr-1 to Gr-7 groups, have been created. All modeled beams had a constant thickness of flange plate out from the used base, I-profile. Each beam group included 4 matching CBs, namely CB-1, CB-2, CB-3, and CB-4 but with only customizing the unbraced length of compression flange (L_b). The lateral unbraced lengths of compression flange $L/2$, $L/4$, $L/8$, and L/∞ were utilized for CB-1, CB-2, CB-3, and CB-4 respectively. The FE results are shown in Figures 10 and 11. Concerning the homogeneous beams, it is obvious from the presented comparisons that using higher-grade steel has increased CBs' failure load for all considered unbraced lengths of compression flange. 60% higher ultimate load has been achieved when using steel grade S460 with $L_b = L/8$ compared to the ultimate load of the same CB with S275 steel grade. The relatively close distance between the provided lateral supports, prevented the compression flange to move perpendicular to the web plate plane. Such lateral restraints have stiffened CBs against failure in the instability lateral-distortional buckling mode. Therefore, the stresses at the critical cross section, mid-span section, reached the material ultimate strength as long as no local buckling was observed during the analysis. Hence, the employed steel grade has a great impact in the final attained ultimate load for CBs with $L_b = L/8$ or $L_b = 0$.

In the case of HCB and relatively nearby lateral restraining points, the beam didn't have any kind of lateral instabilities, either lateral torsional or lateral torsion-distortional buckling. Since the bottom beam's half has a lower steel grade than the top half, the mid-span bottom flange reached the yield stress whereas the top flange was still much below its nominated material's yield stress, as depicted in Figure 12. The analysis of these HCBs with $L_b = L/8$ or $L_b = 0$, was terminated because the mid-span bottom flange reached its ultimate strength. Moreover, stress concentration was recorded at the mid-span opening's corner by achieving the beam's ultimate load. The early failure of HCB with comparatively short L_b before the top flange achieves ultimate stress, demonstrates the grounds of a low ratio of acquired ultimate load shown in Figure 11. Consequently, using higher-grade steel only in the CBT with relatively short L_b, has a rather low impact on the beam's load carrying capacity.

Considering the analyzed CBs with $L_b = L/4$, the beams have failed in the mode of instability lateral-distortional buckling. The ultimate load strength of homogeneous beams with $L/4$ unbraced length, has been achieved as the top flange was fully yielded whereas the bottom flange was partially yielded. Such stress distribution of both beam flanges points out that the employed steel grade has a substantial impact on the beams' ultimate strength, agreeing with the results shown in Figure 10. Furthermore, at the ultimate load of the analyzed HCBs, the mid-span bottom flange, with a lower steel grade, was fully yielded whereas the top flange had limited yielded areas compared to the homogeneous beams. This explicates the relatively low ultimate strength achieved when compared to a commensurate homogenous beam. Also in this case, stress concentration was observed at the top corner of the web opening next to the middle web post of HCB. However, applying relatively distant lateral supporting points to the compressed flange, resulted in a lateral torsion-distortional buckling failure with full yielding of the top flange. Therefore, using higher-grade steel for the CBT delayed HCB's failure and allowed carrying higher load than the homogeneous beam with S275 steel grade. Since the failure of these CBs has commenced before any yielding initiation at the bottom flange, the acquired load strength ratios were indistinguishable for the same utilized higher-grade steel, either in homogenous or in hybrid beams. As a result, higher-grade steel has almost identical effects on the CB gained strength of homogeneous and hybrid beams.

2) Applying Higher Grade Steel to the Flanges of Castellated Beams

In this form of HCBs, higher-grade steel was applied to the beam flanges instead of the top-half part. Three HCB groups, Gr-22, Gr-23, and Gr-24 similar to the earlier presented groups Gr-1, Gr-2, and Gr-3, were created except that material grade S275 was assigned to the beam's web plate, and the higher-grade steel was assigned to the flanges. The values of L_b, i.e. $L/2$, $L/4$, $L/8$, and L/∞ were utilized in 4 beams: CB-1, CB-2, CB-3, and CB-4 in each group. HCB FE models of the flange plate's material grades of S355, S420, and S460 are referred to respectively as Flange_S355, Flange_S420, and Flange_S460. The analysis results are shown in Figure 13. The gained strength using beam flanges with higher-grade steel was close to that obtained from the corresponded homogeneous beams with the same steel grade.

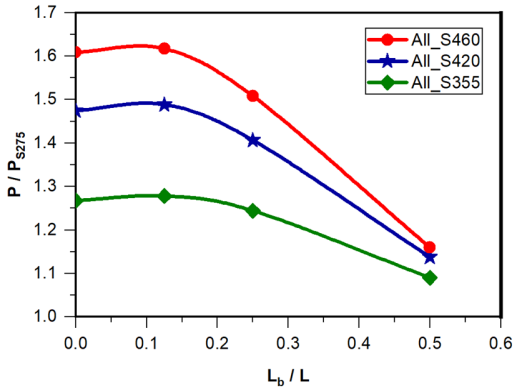

Fig. 10. Ultimate load of homogeneous castellated beams using various steel grades.

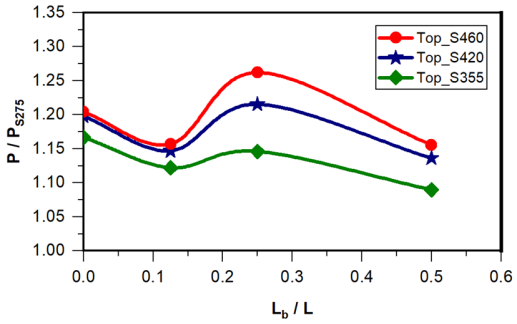

Fig. 11. Ultimate load of hybrid castellated beams, with higher garde steel assigned to the top part of the beam.

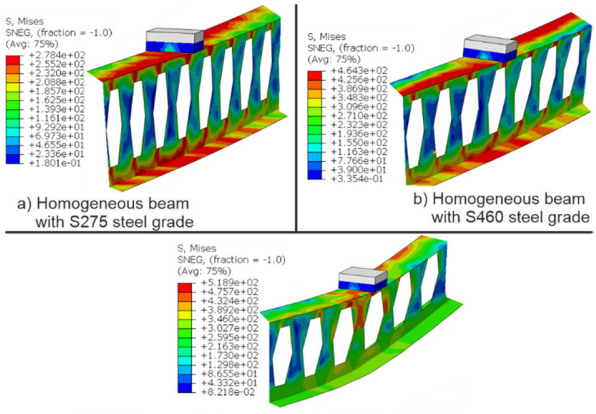

Fig. 12. Von Misses stresses of numerically analyzed beam with $L/4$ unbraced length.

V. ANALYTICAL STUDY

Since castellated beams are deeper and slenderer than the original root I-profile rolled sections, and because of the existing web openings, castellated beams are sensitive to lateral buckling, whether lateral-torsional or lateral-distortional. Such

behavior was dominant in the tested castellated beams and among most of the numerically analyzed beams as well. Therefore, finding out a relation able to predict the inelastic distortional-buckling moment (M_{id}) of simply supported castellated beams loaded with mid-span point load, became essential. Many formulas dealing with buckling of beams with web openings, have focused on determining the elastic lateral-torsional buckling of a simply beam under various load types as provided in [36, 37], whereas castellated beam elastic lateral-torsional and elastic lateral-distortional were analytically determined in [38].

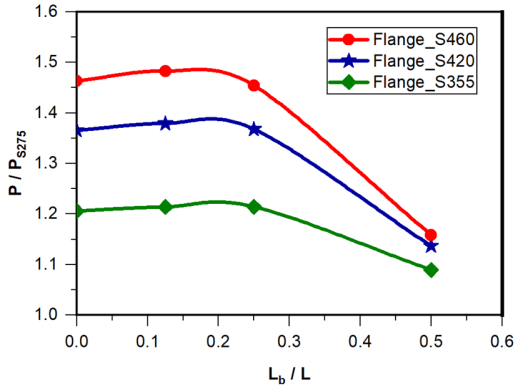

Fig. 13. Failure loads of hybrid symmetric castellated beams considering flanges with various steel grades.

Based on the FE results of the conducted parametric study, the inelastic distortional buckling, M_{id}, of a simply supported castellated beam, whether homogeneous or hybrid, loaded by concentrated load at mid-span can be obtained by:

$$\frac{M_{id}}{M_P} = \frac{\alpha}{R^k} \quad (1)$$

where M_p is the cross-section plastic moment, and α, k are constants equal to 0.77 and 1.6 respectively. R and M_p are given by:

$$R = \sqrt{\frac{M_P}{M_{cr}}}, \quad M_P = F_y\, Z_x \quad (2)$$

where F_y is the yield stress of the homogeneous castellated beam or the yield stress of castellated beam top-half in case of HCB, and Z_x is:

$$Z_x = t_w \left(\frac{h_w^2 - h_a^2}{4}\right) + b_f\, t_f \left(h - t_f\right) \quad (3)$$

The used notations are declared in Figure 14.

The elastic critical distortional moment, M_{cr}, derived by [38], is modified to fulfill the castellated beam case:

$$M_{cr} = C_m \frac{C\pi}{L} \sqrt{E\, I_y\, GJ_e\, (1 + W^2)} \quad (4)$$

$$C_m = 1.36 + 0.02U^2 - 0.171U \quad (5)$$

$$U = \frac{L}{h}\frac{t_f}{b_f} \quad (6)$$

where L is the beam's span length, E is the modulus of elasticity, I_y is the y-axis moment of inertia; C is a coefficient which can be taken as [30]:

$$C = 2.95 - 1.143\, W^2 + 4.07\, W \quad (7)$$

$$W = \frac{\pi}{L}\sqrt{\frac{EC_{we}}{GJ_e}} \quad (8)$$

EC_{we} and GJ_e are the effective warping and torsion rigidities in order.

$$C_{we} = \frac{C_w}{1 + r_{fw}\left(\frac{h}{12L}\right)\left(1 + \frac{b_f}{h}\right)}, \quad r_{fw} = \frac{t_f}{t_w} \leq 2 \quad (9)$$

where C_w is the warping constant. The effective torsion constant, J_e, can be calculated by:

$$J_e = \frac{2\, J_f\, (12 D_w\, L^2)}{(\pi^2 h)} \Big/ \left(2\, G\, J_f + \frac{(12 D_w\, L^2)}{(\pi^2 h)}\right) \quad (10)$$

where J_f is the flange torsion constant and D_w is:

$$D_w = \frac{E\, t_w^3}{12(1 - \nu^2)} \quad (11)$$

where ν is the Poisson ratio = 0.3.

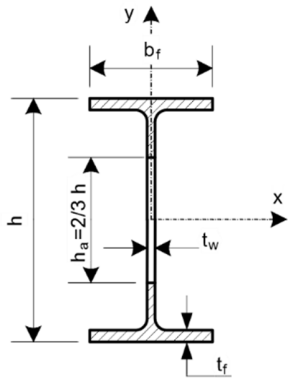

Fig. 14. Cross-section employed notations.

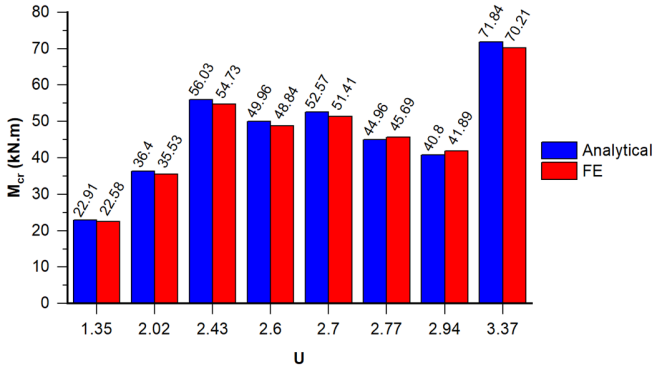

Fig. 15. Elastic critical distortional moment determined by both of modified equation and FE analysis.

M_{cr} in (4), can predict the elastic critical distortional moment to an acceptable precision degree compared to all numerically analyzed CBs with lateral supports at the mid-span and at the end. The closeness of the elastic critical distortional

moment determined by (4), to that obtained numerically, varies from 97.40% to 102.45%. Figure 15 shows the close agreement between the elastic distortional moment of CBs achieved numerically and by (4). Figure 16 presents a comparison between the moment determined by the proposed equation and that evaluated using FE analysis. The comparison conducted in Figure 16, proves that (1) can anticipate, with an acceptable accuracy, the inelastic moment capacity of CB fails in the lateral-distortional buckling mode. Moreover, this equation can be used for both homogeneous and hybrid CBs.

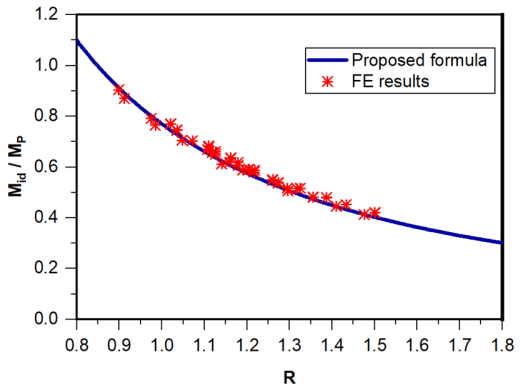

Fig. 16. Inelastic distortional moment from the proposed equation and numerical analysis.

VI. CONCLUSIONS

HCBs formed from two rolled-profiles of varying steel grades, could represent an alternative to strengthen CBs. The current study aimed to find out the advances of HCBs formed from various hot rolled profiles with different steel grades. The close agreement between the results of FE analysis and of experimented CBs, considering both attained ultimate strength and final developed deformations, allowed to employ the developed numerical model in a further parametric study. The conducted parametric study put some light on the influence of specific factors, i.e. slenderness degree of compression flange, beam span-to-depth ratio, and length of unbraced compression flange on the ultimate strength of HCBs. In general, replacing the top-half part of simply supported homogeneous CBs with higher-grade steel, leads to the formation of HCBs with remarkably greater ultimate strength. The carried out numerical analysis has confirmed that applying higher steel grade to the top-half part of CB is more significant when considering a relatively compact top compression flange. The substantially higher proportion of a beam span-to-depth ratio, has a worse effect on the ultimate strength of both CBs and HCBs. Both homogeneous CBs and HCBs with the same steel grade, have an indistinguishable impact on the beam load capacity for all considered values of flange slenderness or beam-span-to-depth ratio.

The L_b of compressed flange has a significant impact on the CB strength. In the view of numerically simulated CBs with L_b less than or equal to $L/4$, the carried-out FE analysis proved that employing a higher-grade material has a positive influence on the beam strength. The maximum load capacities have been achieved in the homogeneous CBs, whereas these load values were shifted down about 10% in the case of higher-grade material assigned to beam's flanges. Compared to the previous two CB types, the minimum acquired ultimate load has been recorded in the case of HCBs with higher-grade steel being employed to CBT. For rather distant lateral restraining points, lateral instabilities were highly expected and the gained load capacities were very close between all analyzed CBs, including HCBs. Therefore, whenever lateral instability of simply supported CB is anticipated, it is recommended to utilize HCBs to raise beam's load capacity up to 25% depending on the beam's geometry and applied transverse restraints.

Based on the results of the carried-out FE analysis, a design formula is proposed to determine the inelastic lateral-distortional beam strength. This formula is limited for simply supported CB with mid-span point load. Furthermore, the compression flange should be provided with transversal restraints at end-supports in addition to a lateral support at mid-span. The proposed equation can determine the load capacity for HCBs and homogeneous CBs. The load strengths determined by the suggested equation are very close to that resulting from FE analysis.

ACKNOWLEDGMENT

The author acknowledges the approval and the support of this research study by the grant no. F-10-1-2019-ENG-8389 from the Deanship of Scientific Research at Northern Border University, Arar, Saudi Arabia.

REFERENCES

[1] M. A. Serna, A. Lopez, I. Puente, and D. J. Yong, "Equivalent uniform moment factors for lateral–torsional buckling of steel members," *Journal of Constructional Steel Research*, vol. 62, no. 6, pp. 566–580, Jun. 2006, https://doi.org/10.1016/j.jcsr.2005.09.001.

[2] H. Veladi and H. Najafi, "Effect of Standard No. 2800 Rules for Moment Resisting Frames on the Elastic and Inelastic Behavior of Dual Steel Systems," *Engineering, Technology & Applied Science Research*, vol. 7, no. 6, pp. 2139–2146, Dec. 2017, https://doi.org/10.48084/etasr.1040.

[3] P. C. Nguyen, B. Le-Van, and S. D. T. V. Thanh, "Nonlinear Inelastic Analysis of 2D Steel Frames : An Improvement of the Plastic Hinge Method," *Engineering, Technology & Applied Science Research*, vol. 10, no. 4, pp. 5974–5978, Aug. 2020, https://doi.org/10.48084/etasr.3600.

[4] N. L. Tran and T. H. Nguyen, "Reliability Assessment of Steel Plane Frame's Buckling Strength Considering Semi-rigid Connections," *Engineering, Technology & Applied Science Research*, vol. 10, no. 1, pp. 5099–5103, Feb. 2020, https://doi.org/10.48084/etasr.3231.

[5] E. H. Mehr and H. R. Saba, "Ductility Evaluation of Steel Structures with Reduced Beam Sections and Post-Tensioned Cables Using the Finite Element Method," *Engineering, Technology & Applied Science Research*, vol. 7, no. 6, pp. 2236–2239, Dec. 2017, https://doi.org/10.48084/etasr.1568.

[6] K. F. Chung, T. C. H. Liu, and A. C. H. Ko, "Investigation on Vierendeel mechanism in steel beams with circular web openings," *Journal of Constructional Steel Research*, vol. 57, no. 5, pp. 467–490, May 2001, https://doi.org/10.1016/S0143-974X(00)00035-3.

[7] S. Durif, A. Bouchair, and O. Vassart, "Experimental tests and numerical modeling of cellular beams with sinusoidal openings," *Journal of Constructional Steel Research*, vol. 82, pp. 72–87, Mar. 2013, https://doi.org/10.1016/j.jcsr.2012.12.010.

[8] A. H. Gandomi, S. M. Tabatabaei, M. H. Moradian, A. Radfar, and A. H. Alavi, "A new prediction model for the load capacity of castellated steel beams," *Journal of Constructional Steel Research*, vol. 67, no. 7, pp. 1096–1105, Jul. 2011, https://doi.org/10.1016/j.jcsr.2011.01.014.

[9] S. G. Morkhade and L. M. Gupta, "An experimental and parametric study on steel beams with web openings," *International Journal of Advanced Structural Engineering*, vol. 7, no. 3, pp. 249–260, Sep. 2015, https://doi.org/10.1007/s40091-015-0095-4.

[10] M. Najafi and Y. C. Wang, "Behaviour and design of steel members with web openings under combined bending, shear and compression," *Journal of Constructional Steel Research*, vol. 128, pp. 579–600, Jan. 2017, https://doi.org/10.1016/j.jcsr.2016.09.011.

[11] P. D. Pachpor, L. M. Gupta, and N. V. Deshpande, "Analysis and Design of Cellular Beam and its Verification," *IERI Procedia*, vol. 7, pp. 120–127, Jan. 2014, https://doi.org/10.1016/j.ieri.2014.08.019.

[12] P. Sivak, I. Delyova, and T. Kaluja, "Determining the strength properties of castellated girders by experimental and numerical modeling," in *55th International Conference on Experimental Stress Analysis*, Novy Smokovec, Slovakia, Jun. 2017, pp. 534–542.

[13] M. A. Gizejowski and W. A. Salah, "Numerical Modeling of Composite Castellated Beams," in *International Conference on Composite Construction in Steel and Concrete*, Tabernash, CO, USA, Jul. 2008, pp. 554–565, https://doi.org/10.1061/41142(396)45.

[14] D. Kerdal and D. A. Nethercot, "Failure modes for castellated beams," *Journal of Constructional Steel Research*, vol. 4, no. 4, pp. 295–315, Jan. 1984, https://doi.org/10.1016/0143-974X(84)90004-X.

[15] J. Megharief and R. Redwood, "Behaviour of composite castellated beams," *Journal of Constructional Steel Research*, vol. 46, no. 1, pp. 199–200, Apr. 1998, https://doi.org/10.1016/S0143-974X(98)80019-9.

[16] M. R. Soltani, A. Bouchair, and M. Mimoune, "Nonlinear FE analysis of the ultimate behavior of steel castellated beams," *Journal of Constructional Steel Research*, vol. 70, pp. 101–114, Mar. 2012, https://doi.org/10.1016/j.jcsr.2011.10.016.

[17] A. J. Wang and K. F. Chung, "Advanced finite element modelling of perforated composite beams with flexible shear connectors," *Engineering Structures*, vol. 30, no. 10, pp. 2724–2738, Oct. 2008, https://doi.org/10.1016/j.engstruct.2008.03.001.

[18] M. M. Sehwail, "Lateral Torsional Buckling of Steel I-Section Cellular Beams," Ph.D. dissertation, Eastern Mediterranean University, Famagusta, Cyprus, 2013.

[19] D. Sonck and J. Belis, "Weak-axis flexural buckling of cellular and castellated columns," *Journal of Constructional Steel Research*, vol. 124, pp. 91–100, Sep. 2016, https://doi.org/10.1016/j.jcsr.2016.05.002.

[20] K. D. Tsavdaridis and C. D'Mello, "Web buckling study of the behaviour and strength of perforated steel beams with different novel web opening shapes," *Journal of Constructional Steel Research*, vol. 67, no. 10, pp. 1605–1620, Oct. 2011, https://doi.org/10.1016/j.jcsr.2011.04.004.

[21] W. Zaarour and R. Redwood, "Web Buckling in Thin Webbed Castellated Beams," *Journal of Structural Engineering*, vol. 122, no. 8, pp. 860–866, Aug. 1996, https://doi.org/10.1061/(ASCE)0733-9445(1996)122:8(860).

[22] T. Zirakian and H. Showkati, "Distortional buckling of castellated beams," *Journal of Constructional Steel Research*, vol. 62, no. 9, pp. 863–871, Sep. 2006, https://doi.org/10.1016/j.jcsr.2006.01.004.

[23] F. Ahmad and N. Zoubi, "Tension field action behavior in the hybrid steel girders for Ohio approach spans of Blennerhassett Island Bridge," *Bridge Structures*, vol. 1, no. 3, pp. 211–221, Sep. 2005, https://doi.org/10.1080/15732480500247421.

[24] A. Azizinamini, J. B. Hash, A. J. Yakel, and R. Farimani, "Shear Capacity of Hybrid Plate Girders," *Journal of Bridge Engineering*, vol. 12, no. 5, pp. 535–543, Sep. 2007, https://doi.org/10.1061/(ASCE)1084-0702(2007)12:5(535).

[25] M. Bock, R. Chacon, E. Mirambell, and E. Real, "Hybrid steel plate girders subjected to patch loading," *Steel Construction*, vol. 5, no. 1, pp. 3–9, 2012, https://doi.org/10.1002/stco.201200001.

[26] N. Greco and C. J. Earls, "Structural Ductility in Hybrid High Performance Steel Beams," *Journal of Structural Engineering*, vol. 129, no. 12, pp. 1584–1595, Dec. 2003, https://doi.org/10.1061/(ASCE)0733-9445(2003)129:12(1584).

[27] M. Veljkovic and B. Johansson, "Design of hybrid steel girders," *Journal of Constructional Steel Research*, vol. 60, no. 3, pp. 535–547, Mar. 2004, https://doi.org/10.1016/S0143-974X(03)00128-7.

[28] C. S. Wang, L. Duan, M. Wei, L. X. Liu, and J. Y. Hu, "Bending Behavior of Hybrid High Performance Steel Beams," *Advanced Materials Research*, vol. 163–167, pp. 492–495, 2011, https://doi.org/10.4028/www.scientific.net/AMR.163-167.492.

[29] R. C. Haddock and Z. Razzaq, "Calculating Bending Stresses in an Unsymmetrical Hybrid Beam," *Practice Periodical on Structural Design and Construction*, vol. 14, no. 4, pp. 214–218, Nov. 2009, https://doi.org/10.1061/(ASCE)1084-0680(2009)14:4(214).

[30] A. S. Kulkarni and L. M. Gupta, "Experimental Investigation on Flexural Response of Hybrid Steel Plate Girder," *KSCE Journal of Civil Engineering*, vol. 22, no. 7, pp. 2502–2519, Jul. 2018, https://doi.org/10.1007/s12205-017-0313-7.

[31] J. Chroscielewski, Z. Cywinski, and W. Smolenski, "Postbuckling behaviour of hybrid plate girders with web openings," *Journal of Constructional Steel Research*, vol. 18, no. 2, pp. 165–170, Jan. 1991, https://doi.org/10.1016/0143-974X(91)90071-8.

[32] J. Chroscielewski, Z. Cywinski, and A. Sitarski, "Conventional and advanced bending strength analysis of common and castellated, homogeneous and hybrid I-beams," *Stahlbau*, vol. 81, no. 2, pp. 142–150, 2012, https://doi.org/10.1002/stab.201201511.

[33] M. Smith, *ABAQUS/Standard User's Manual, Version 6.14*. Providence, RI, USA: Dassault Systèmes Simulia Corp, 2014.

[34] S. Chen and Y. Jia, "Numerical investigation of inelastic buckling of steel–concrete composite beams prestressed with external tendons," *Thin-Walled Structures*, vol. 48, no. 3, pp. 233–242, Mar. 2010, https://doi.org/10.1016/j.tws.2009.10.009.

[35] *BS EN 1993-1-3(2006), Eurocode 3 Design of steel structures Part 1-3: General rules Supplementary rules for cold-formed members and sheeting*. London, UK: British Standards Institution, 2006.

[36] S. Elaiwi, B. Kim, and L.-Y. Li, "Bending Analysis of Castellated Beams," *Athens Journal of Technology & Engineering*, vol. 6, no. 1, pp. 1–16, Feb. 2019, https://doi.org/10.30958/ajte.6-1-1.

[37] B. Kim, L.-Y. Li, and A. Edmonds, "Analytical Solutions of Lateral–Torsional Buckling of Castellated Beams," *International Journal of Structural Stability and Dynamics*, vol. 16, no. 08, Oct. 2016, Art. no. 1550044, https://doi.org/10.1142/S0219455415500443.

[38] I. Kalkan and A. Buyukkaragoz, "A numerical and analytical study on distortional buckling of doubly-symmetric steel I-beams," *Journal of Constructional Steel Research*, vol. 70, pp. 289–297, Mar. 2012, https://doi.org/10.1016/j.jcsr.2011.06.006.

[39] D. Sonck and J. Belis, "Lateral-Torsional Buckling Resistance of Castellated Beams," *Journal of Structural Engineering*, vol. 143, no. 3, Mar. 2017, Art. no. 04016197, https://doi.org/10.1061/(ASCE)ST.1943-541X.0001690.